



## Highly Efficient Bromine Capture and Storage Using N-containing Porous Organic Cages

Journal:	<i>Journal of Materials Chemistry A</i>
Manuscript ID	TA-ART-07-2022-005420.R2
Article Type:	Paper
Date Submitted by the Author:	20-Oct-2022
Complete List of Authors:	Lee, Sunggyu; Korea Advanced Institute of Science and Technology, Chemical and Biomolecular Engineering Kevlishvili, Ilia ; Massachusetts Institute of Technology Kulik, Heather; Massachusetts Institute of Technology, Chemical Engineering Kim, Hee-Tak; KAIST, Department of Chemical & Biomolecular Engineering Chung, Yongchul; Pusan National University, Chemical Engineering Koh, Dong-Yeun; Korea Advanced Institute of Science and Technology, Chemical and Biomolecular Engineering

# Highly Efficient Bromine Capture and Storage Using N-containing Porous Organic Cages

Sunggyu Lee<sup>1,#</sup>, Iliia Kevlishvili<sup>2,#</sup>, Heather J. Kulik<sup>2</sup>, Hee-Tak Kim<sup>1,4</sup>, Yongchul G. Chung<sup>3\*</sup>,  
Dong-Yeun Koh<sup>1,4\*</sup>

<sup>1</sup>Department of Chemical and Biomolecular Engineering (BK21 Four), Korea Advanced Institute of Science and Technology, Daejeon, 34141, South Korea

<sup>2</sup>Department of Chemical Engineering, Massachusetts Institute of Technology, Cambridge, Massachusetts 02139, United States

<sup>3</sup>School of Chemical Engineering, Pusan National University, Busan 46241, South Korea

<sup>4</sup>KAIST Institute for NanoCentury, Daejeon, 34141, South Korea

## Abstract

Highly volatile and toxic bromine ( $\text{Br}_2$ ) molecules can be utilized safely in various chemical processes when coupled with efficient separation systems. Herein, we present two different N-containing porous organic cages (POCs), Covalent Cage 3-R (CC3-R) and Formaldehyde Tied-Reduced Covalent Cage 3 (FT-RCC3), for vapor  $\text{Br}_2$  capture under ambient conditions. They show outstanding sorption capacities (11.02 mmol/g and 11.64 mmol/g, respectively) compared with previously reported adsorbents. Reversibility of the  $\text{Br}_2$  sorption process has been elucidated experimentally and computationally by identifying bromine species adsorbed at POCs and calculating their binding energies. The strong charge-transfer interactions between adsorbed  $\text{Br}_2$  and abundant N atomic sites of the host cages led to the dominant formation of polybromide species ( $\text{Br}_3^-$ ,  $\text{Br}_5^-$ ). Further host-guest interaction between POCs and polybromides determined the reversibility of the  $\text{Br}_2$  sorption process—showing partially

reversible ( $> 70\%$  recovery) behavior for CC3-R and irreversible ( $< 10\%$  recovery) behavior for FT-RCC3, both of which were affected by the chemical and structural nature of different POCs. DFT calculations further indicate that the formation of carbocationic species ( $\text{Br}_3^-$  and  $\text{Br}_5^-$ ) and HBr is energetically favorable within the cage, which are in good agreement with experimental results. This work demonstrates that strong host-guest interactions are essential for highly efficient  $\text{Br}_2$  capture and storage performance.

## 1 Introduction

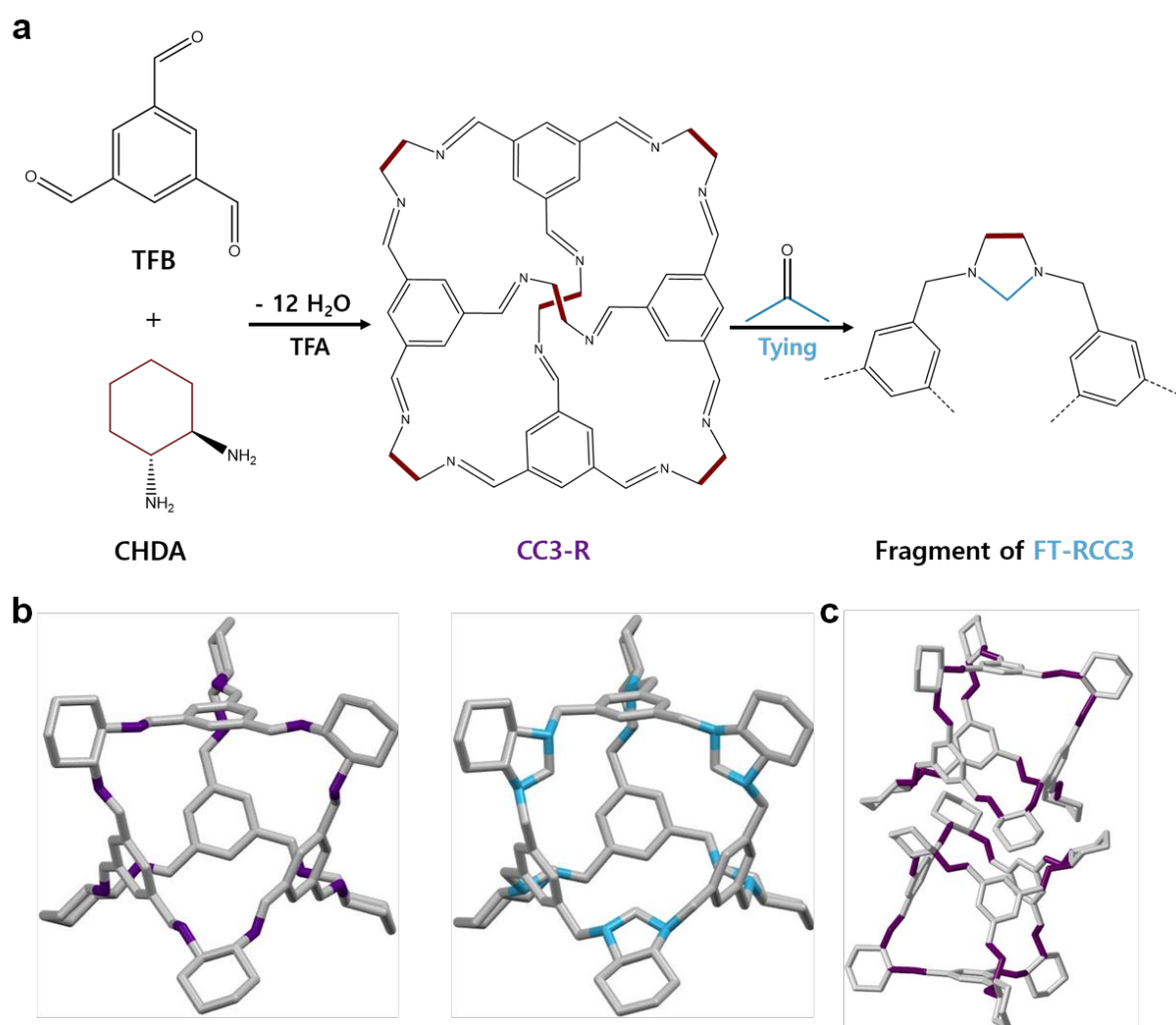
The diverse reactivity of bromine ( $\text{Br}_2$ ), such as charge compensating anions in cross-coupling reactions and  $\text{S}_{\text{N}}2$  reactions, is widely used in the industry to produce chemical intermediates and pharmaceuticals. However, the utility of bromine in the chemical industry is largely limited by its severe toxicity, corrosiveness, and volatility, which poses a significant safety concern for the chemical process operation. The high energy density provided by the bromine redox process in Zn-Br batteries (ZBBs) has been proposed for their low-cost energy storage system (ESS) operation.<sup>1, 2</sup> However, the large-scale deployment of the ZBB face significant hurdles due to the build-up of battery stack pressure which might induce leakage of  $\text{Br}_2$  into the atmosphere. Toward this end, a small and efficient adsorption-based separation system capable of capturing bromine molecules could accelerate the deployment of ZBB system. Adsorption-based separation systems provide advantages such as a small device footprint, easy operation, and low energy usage. Until now, only a few adsorbent materials, such as cobalt- or zirconium-based metal-organic frameworks<sup>3</sup> and vacancy-ordered perovskites,<sup>4</sup> have been investigated for the adsorptive capture of  $\text{Br}_2$ . New porous adsorbents with high capacity, potential scalability, and chemical stability to  $\text{Br}_2$  are highly desirable for capturing  $\text{Br}_2$  under ambient conditions which can contribute to the safe handling of the hazardous chemicals.

Halogen compounds, frequently used as electron acceptors, have a good affinity for electron-donating groups. Extensive research into the capture of iodine ( $\text{I}_2$ ) has discovered that electron-rich adsorbents would successfully adsorb electron-deficient iodine molecules by forming charge-transfer complexes.<sup>5-7</sup> According to a recent study, ionic functionalized covalent organic frameworks (iCOFs), incorporating abundant binding sites with high electron densities, developed for  $\text{I}_2$  capture performed exceptionally well in adsorption capacity and kinetics.<sup>8</sup> The binding sites of iCOFs, including imine, triazine moieties, and cationic sites, would be attributed to their high adsorption capacity by charge-transfer and coulombic

interactions with I<sub>2</sub>. Br<sub>2</sub> could also preferentially interact with electron-rich species such as imine, triazine, etc. For example, a computational study shows that Br<sub>2</sub> interacts strongly with the electron-donating nitrogen atom from amine functional groups via charge-transfer interaction.<sup>9</sup> Based on these studies, porous adsorbent materials with rich N atoms per volume could be effective for Br<sub>2</sub> capture.

Porous organic cages (POCs) are a new subclass of porous materials with inherent ultramicroporous discrete cages that can be packed together to produce a three-dimensional uniform pore network. POCs have been primarily explored in applications including gas storage,<sup>10a</sup> molecular sensor,<sup>10b</sup> catalyst support,<sup>10c</sup> shape-selective chromatography for aromatic isomers separation,<sup>10d</sup> etc. CC3-R, also known as imine-based POCs (**Scheme 1a**), has shown potential for adsorptive removal of acidic gases<sup>11a</sup> or radioisotope pollutants<sup>11b</sup> due to rich N atoms on the frameworks (14.3% in unit cell atomic composition). Their crystallographic information was also investigated by using single crystal X-ray diffractometers.<sup>11b</sup> Post-synthetic modifications on CC3-R could further alter the internal cavity size and shape at the atomic level without impacting the chemical composition or crystal packing.<sup>12a</sup> FT-RCC3, a “tied” POC formed by reactions of imine groups in CC3-R with aldehydes (**Scheme 1a**), has proved to be highly stable in acidic and basic environments.<sup>12b</sup> According to recent research, these POCs can be scaled up using various methods, including batch synthesis,<sup>13a</sup> flow synthesis,<sup>13b</sup> microwave-assisted synthesis,<sup>13c</sup> and twin-screw extrusion.<sup>13d</sup> Herein, we use two distinct N-containing POCs (CC3-R and FT-RCC3) to effectively capture bromine vapor under ambient conditions. CC3-R can be constructed from 1,3,5-triformylbenzene (TFB) and (1R,2R)-cyclohexane-1,2-diamine (CHDA), where the [4 + 6] cyclo-condensation reaction of the primary amines and aldehydes results in the formation of the discrete molecular cage through imine linkages (**Scheme 1**). FT-RCC3 can be readily prepared by reducing the imine group of CC3-R followed by the “tying” method with

formaldehyde. Both cages are isostructural as tetrahedral space groups, and their crystal structures formed by window-to-window packing have a three-dimensional diamondoid pore network (**Scheme 1b** and **c**). We illustrate the excellent bromine adsorption capacity and kinetics of the CC3-R and FT-RCC3 (11.41 mmol/g and 10.08 mmol/g, respectively) under static adsorption conditions at room temperature. The drive behind the superior bromine adsorption onto the micropores of the POCs was identified to be the formation of strong charge-transfer complexes either with imine or tertiary amine sites. DFT calculations elucidated the evolution of polybromide species ( $\text{Br}_3^-$ ,  $\text{Br}_5^-$ ) when bromine vapors are adsorbed and stabilized



**Scheme 1** (a) Synthetic procedure of CC3-R and FT-RCC3. (b) Cage structures of CC3-R (left) and FT-RCC3 (Right). Carbons are shown in grey; Imine and tertiary amine are shown in purple and light blue; Hydrogen atoms are omitted for clarity. (c) Schematic illustration of window-to-window packing in the crystal structure of POCs.

in the POCs. The degree of the stability offered by distinct N-groups determined the reversibility of the Br<sub>2</sub> capture process utilizing POCs

## 2 Experimental

### 2.1 Materials and methods

**Materials.** All starting materials and solvents were obtained from commercial sources and used without further purification. Anhydrous dichloromethane (DCM, >99%), 1,3,5-triformylbenzene (TFB, 98%), potassium iodide (KI, 99.5%) were purchased from TCI. Trifluoroacetic acid (TFA, 99%), (1R,2R)-cyclohexane-1,2-diamine (CHDA, 98%), sodium thiosulfate pentahydrate (99.5%) and paraformaldehyde (96%) were purchased from Alfa Aesar.

**Preparation of Porous Organic Cages (POCs).** CC3-R and FT-RCC3 were prepared as previously reported in its homochiral form.<sup>12b, 14</sup> The detailed synthetic procedures are described in the Electronic Supplementary Information (ESI†).

**Static bromine vapor capture.** The static bromine vapor capture was conducted using the customized system,<sup>3a</sup> shown as a photograph in the **Figure S4†**. ~250 mg of activated POCs were loaded in a glass tube that was connected (via a U-shaped glass adapter) to another tube equipped with a Teflon valve. The empty glass tube was filled with liquid Br<sub>2</sub> and tightly closed with the Teflon valve. The system was then evacuated and kept under static vacuum. The Teflon valve sealing the bromine-containing tube was then opened letting the bromine vapors fill the POC-containing tube. The POC was exposed to bromine vapors for certain times, after

which the bromine-containing tube was again sealed by the screw-cap. Excess bromine was then removed under vacuum.

**Measurement of bromine uptake capacity.** The bromine uptake capacity was measured using two kinds of methods; the weight increment of the POCs and iodometric titration method. The static bromine vapor uptake capacity ( $q_t$ ,  $\text{mmol}\cdot\text{g}^{-1}$ ) at certain time was calculated with the following equation (1):

$$q_t = \frac{(m_t - m_0)/M_{w,Br_2}}{m_0}, \quad (1)$$

where  $q_t$  ( $\text{mmol}\cdot\text{g}^{-1}$ ) denotes the static bromine vapor capture capacity at time  $t$ ,  $m_t$  (g) denotes the weight of the glass tube containing POCs at time  $t$ ,  $m_0$  (g) denotes the weight of the glass tube containing POCs before adsorption,  $M_{w,Br_2}$  ( $\text{g}\cdot\text{mol}^{-1}$ ) denotes the molecular weight of bromine. The measurement of bromine uptake capacity using gravimetric method was repeated 2 – 3 times at each adsorption time point.

The experimental procedure of titration method was performed as previously reported.<sup>3a</sup> For measurement of bromine uptake capacity using titration method, captured bromine was desorbed and trapped at the storage flask. The glass tube containing  $\text{Br}_2@\text{POC}$  was connected to a storage flask equipped with a Teflon screw-cap. Before the desorption procedure, the system was evacuated and kept under static vacuum. The glass tube containing  $\text{Br}_2@\text{POC}$  was enclosed by heating wire controlled by a heat controller, while the storage flask was immersed in a Dewar flask filled with liquid  $\text{N}_2$ . The temperature of the heating wire was then gradually raised from room temperature to 200 °C and kept 200 °C for 8 hours under dynamic vacuum conditions. Evolved  $\text{Br}_2$  was trapped in the cooled storage flask. At the end of time, the storage flask was tightly sealed and allowed to warm up to room temperature. The amounts of trapped  $\text{Br}_2$  was determined by iodometric titration. A short glass tube was



connected to the outlet joint of the storage flask. The resulting space (joint + the tube) was filled with an aqueous solution of KI (10% w/v). The Teflon cap was then quickly opened and closed, sucking some of the solution into the bromine-containing flask. The resulting solution was then titrated with 0.2 M aqueous solution of  $\text{Na}_2\text{S}_2\text{O}_3$  (2 eq. of  $\text{Na}_2\text{S}_2\text{O}_3$  for 1 eq. of  $\text{Br}_2$ ). Soluble starch indicator (obtained by boiling 0.1 g of starch in 20 mL of water) was added towards the end of the titration, to allow easier determination of the titration end point.

## 2.2 Characterization methods

Attenuated total reflectance Fourier transform infrared spectra were collected by Nicolet iS50, spectrometer under transmittance mode. The wavenumber range was set from  $500\text{ cm}^{-1}$  to  $4000\text{ cm}^{-1}$  with a resolution of  $4\text{ cm}^{-1}$ . High resolution SEM imaging of POC crystal structures was achieved by FEI Magellan<sup>TM</sup> 400. Powder X-ray Diffraction (PXRD) patterns were measured on RIGAKU SmartLab X-ray diffractometer with Cu  $K\alpha$  radiation ( $\lambda = 1.5406\text{ \AA}$ ) in a range 2-theta of  $5^\circ - 40^\circ$  with a step of  $0.2^\circ$ . Liquid  $^1\text{H}$  NMR spectra in  $\text{CDCl}_3$  were recorded at 600MHz. Solid-state  $^{13}\text{C}$  CPMAS NMR spectra were recorded at 150.95 MHz at spinning rate of 30 kHz.  $^{13}\text{C}$  CPMAS NMR conditions for  $^1\text{H}$ - $^{13}\text{C}$  polarization experiment used a  $\pi/2$  pulse of 2.5  $\mu\text{s}$ , contact time of 2 ms, delay time of 5 s, and 1024 scans. Chemical shifts were referenced to a solid shift at 38.95 ppm relative to TMS. All NMR spectra was collected by using the Bruker Avance Neo 600 spectrometer. X-ray Photoelectron Spectroscopy (XPS) spectra were collected in a Sigma Probe spectrometer, equipped with a monochromatic Al  $K\alpha$  X-ray source ( $h\nu = 1486.7\text{ eV}$ ) at ultra-high vacuum. Nitrogen ( $\text{N}_2$ ) sorption isotherms at 77 K were measured by a volumetric method using a Micromeritics ASAP 2020 gas sorption analyzer. BET (Brunauer-Emmett-Teller) areas was calculated from  $\text{N}_2$  isotherms collected at 77 K. Evolved Gas Analysis (EGA) were performed using NETZSCH STA-GC-MS under an ultra-high purity (UHP) argon flow. The samples were heated up from  $80\text{ }^\circ\text{C}$  to  $800\text{ }^\circ\text{C}$  with

heating rate of 10 °C/min. Raman spectra were recorded using LabRAM HR Evolution Visible\_NIR Raman spectrometer with 514nm laser. Elemental compositions were measured by ZSX Primus II X-ray Fluorescence Spectrometer (XRF) and FlashEA 1112 Elemental Analyzer (EA).

### 3 Results and discussion

#### 3.1 Structural characterization of CC3-R and FT-RCC3

Powder X-ray diffraction (PXRD) and scanning electron microscopy (SEM) was used to check the structural integrity of the POCs as they were synthesized. Both N-containing POCs were highly crystalline, as indicated by PXRD, and these patterns were in good agreement with the simulated structure (**Fig. 1a** and **1b**). POC crystals had highly ordered octahedral structures assembled by window-to-window packing, as seen by SEM images (**Fig. 1c** and **1d**), and this packing was unaffected by the formaldehyde post-synthetic modification. To further verify the successful synthesis and transformation of POCs, we carried out additional analyses, including Fourier transform infrared spectroscopy (FT-IR), <sup>1</sup>H/<sup>13</sup>C nuclear magnetic resonance (NMR) spectroscopy, and X-ray photoelectron spectroscopy (XPS). FT-IR spectra showed a characteristic -C=N- stretching band (1643 cm<sup>-1</sup>) derived from the imine linkage of CC3-R without the appearance of a characteristic band of amino groups (3342 cm<sup>-1</sup>) and aldehyde groups (1690 cm<sup>-1</sup>) from CHDA and TFB (**Fig. 1e** and **Fig. S1†**). These findings demonstrated that TFB and CHDA had undergone a complete Schiff-base reaction. Meanwhile, an additional characteristic aliphatic C-H stretching band at 2794 cm<sup>-1</sup> and the disappearance of the -C=N- stretching band (1643 cm<sup>-1</sup>) in the FT-IR spectrum of FT-RCC3 indicated that formaldehyde had been successfully connected with the parent imine cage via post-synthetic modification. Solid-state <sup>13</sup>C cross-polarization magic angle spinning (CPMAS) NMR and XPS spectra further confirmed this result, which showed an additional aliphatic signal at 79.3 ppm

associated with “tied” groups (-NCH<sub>2</sub>N-) and the binding energy of tertiary amine at 398.40 eV and 399.09 eV (Fig. S2 and S3†). Additionally, the textural properties of the as-synthesized

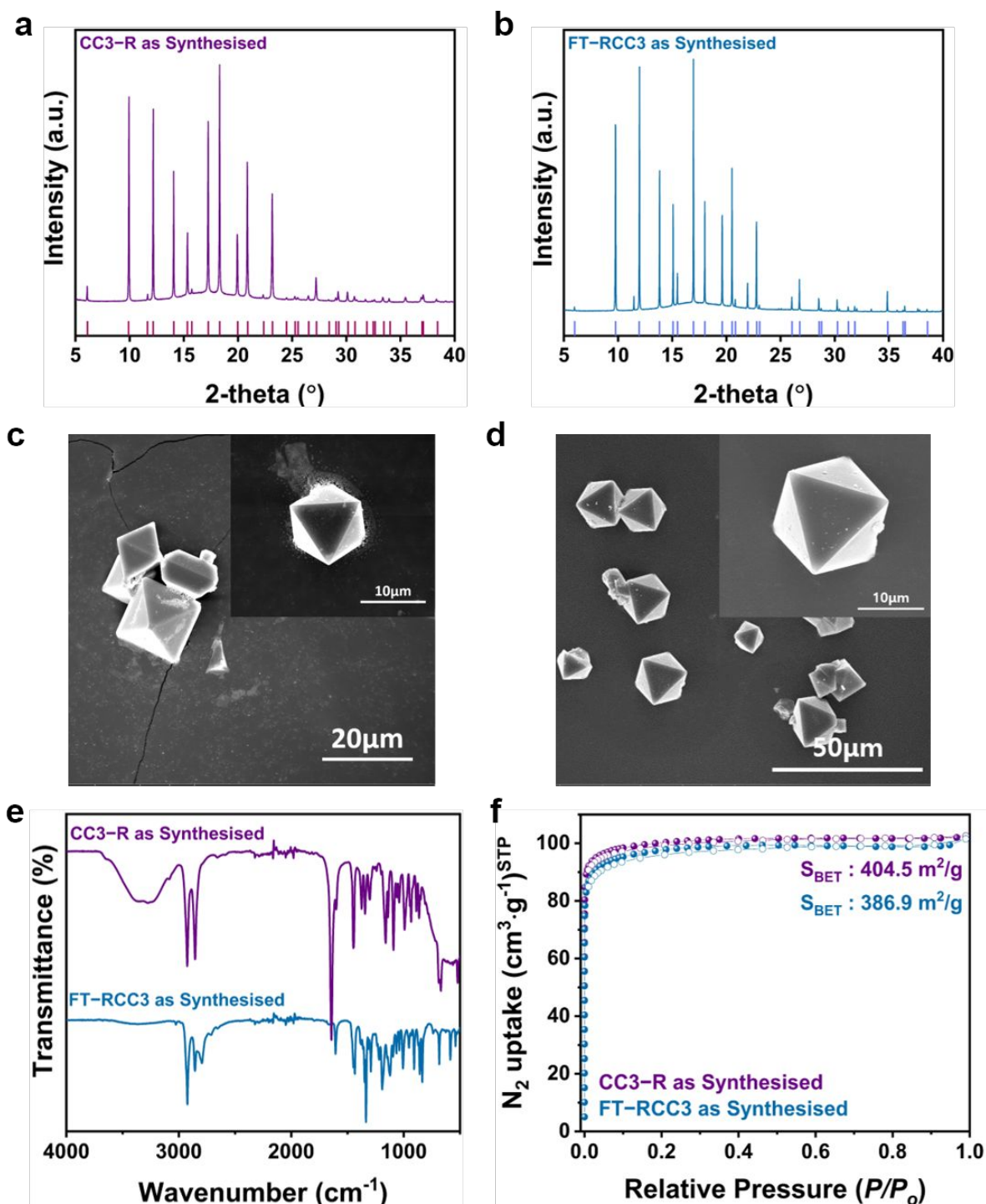


**Fig. 1** Structural characterization of CC3-R and FT-RCC3. PXRD patterns of (a) CC3-R and (b) FT-RCC3. Simulated peaks are shown as below tick marks. SEM images of (c) CC3-R and (d) FT-RCC3. Inset images represent high-resolution images. (e) FT-IR spectra of CC3-R and FT-RCC3. (f) N<sub>2</sub> sorption isotherms of CC3-R and FT-RCC3.

POCs were analyzed with the N<sub>2</sub> physisorption at 77K. Both POCs showed Type I N<sub>2</sub> physisorption isotherms at 77K, indicating their inherent ultramicroporous structures (**Fig. 1f** and **Table S1†**). FT-RCC3 had a lower Brunauer-Emmett-Teller (BET) specific surface area and lower total pore volume than CC3-R due to the tying of the internal cavity.

### 3.2 Static Br<sub>2</sub> adsorption performance of CC3-R and FT-RCC3

We measured the vapor Br<sub>2</sub> adsorption capacities and uptake curves of N-containing POCs (CC3-R and FT-RCC3) under ambient, static conditions (25°C and 0.3 bar of Br<sub>2</sub> vapor pressure). The experimental setup is shown in **Fig. S4†**. Based on the gravimetric measurements, CC3-R and FT-RCC3 exhibited high Br<sub>2</sub> adsorption capacities of 9.49 and 9.71 mmol/g in the first 24 hours of adsorption, respectively; 11.02 mmol/g and 11.64 mmol/g in the first 48 hours of adsorption, respectively (**Fig. 2a** and **2b**). They outperformed the Br<sub>2</sub> adsorption capacity (4 – 70 times) of previously reported adsorbents<sup>3a, 15</sup> (**Table S1†**). The high capture performance would be attributed to their large number of N atoms per discrete molecular cage (14.3% of unit cell atomic composition). Additionally, these values are higher when compared to calculated adsorption capacities from the GCMC simulation<sup>25</sup> (**Table S9†**). As the molecular simulation snapshots (**Figure S34†**) indicated, a single Br<sub>2</sub> is adsorbed inside each cage while the channels connecting the cages are occupied by a single Br<sub>2</sub> molecule. The discrepancy between the simulated and experimental saturation uptake is likely a combination of the formation of polybromide species (further discussed in the following sections) and the expansion of cage-to-cage channel distance which could contribute to the additional adsorption sites for Br<sub>2</sub> molecules. Notably, FT-RCC3 showed faster adsorption kinetics than CC3-R. These findings suggest that tertiary amine groups interact with bromine molecules more favorably than imine groups, which is in line with earlier research<sup>9a</sup>; additionally, the equilibrium sorption capacities were affected by the total pore volume and BET surface area

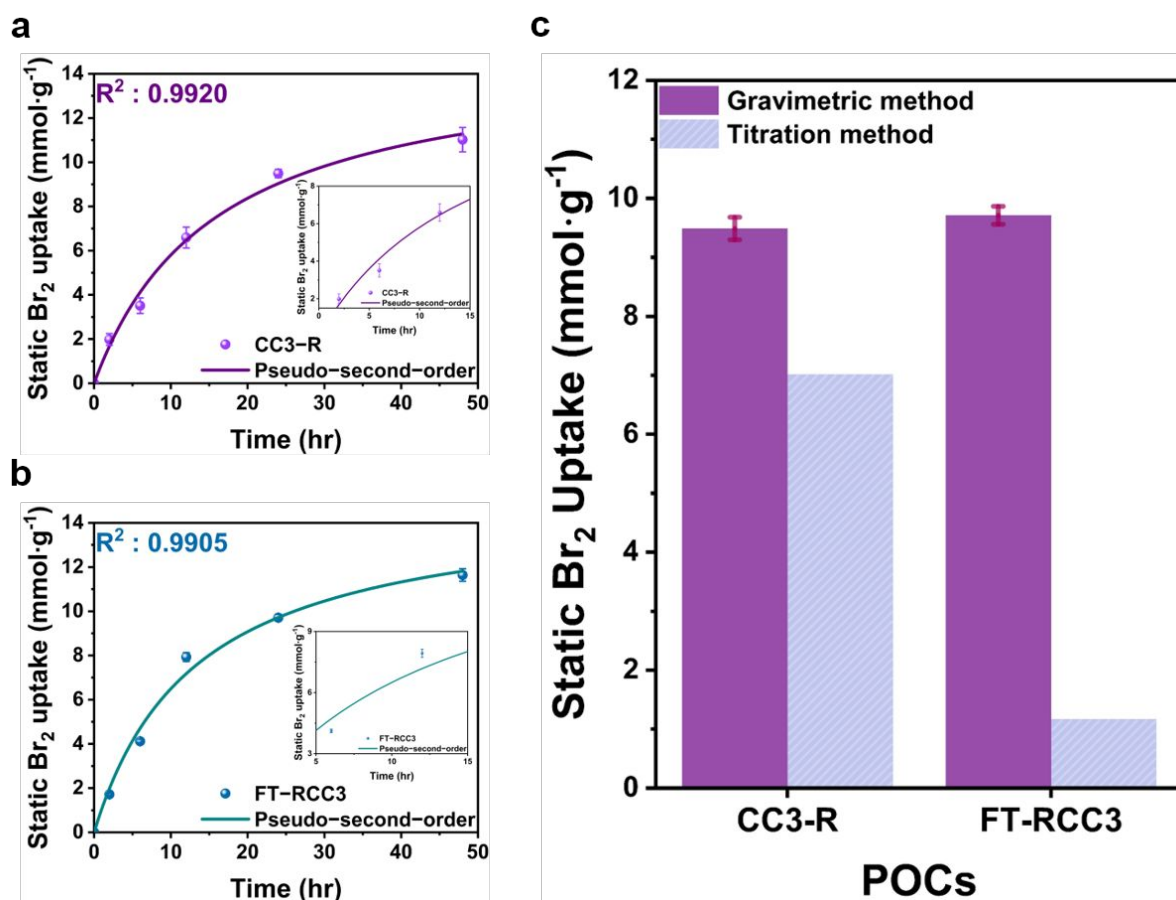


**Fig. 2** Static Br<sub>2</sub> adsorption performance. Gravimetric measurement of static Br<sub>2</sub> vapor uptake capacities of (a) CC3-R and (b) FT-RCC3 as a function of time at 25°C and near ambient pressure. (c) Comparison of static Br<sub>2</sub> capture capacities over 24 hours based on the measurement methods. The error bar represents the variation in Br<sub>2</sub> uptake with 2 - 3 replicated experiments at each adsorption time point. Inset images were magnification parts of multiple adsorption points for verifying the error bars.

of these materials (Table S1†). Furthermore, the adsorption kinetic curves of both POCs (Fig. 2 and Fig. S5†) were well-matched with a pseudo-second-order adsorption model (R-square values of CC3-R and FT-RCC3 are 0.9920 and 0.9905, respectively) showing that the adsorption rate is regulated by a chemical reaction between bromine molecules and POC frameworks.<sup>16</sup> Interestingly, the variations in uptake capacities evaluated by two different methods (gravimetric versus titration) were greater in FT-RCC3 than in CC3-R, indicating stronger irreversible chemisorption occurring in FT-RCC3 (Fig. 2c). The titration was performed using the collected Br<sub>2</sub> after the thermal desorption of the bromine from the POCs,

and the adsorption capacity calculated from the gravimetric method was higher than that of the titration method due to the existence of a small portion of the condensed Br<sub>2</sub> phase. CC3-R with abundant imine sites showed partially-reversible sorption of Br<sub>2</sub> with the recovery of Br<sub>2</sub> by thermal desorption (> 100 – 200°C) was observed up to 70%. While FT-RCC3 with sterically hindered tertiary amine sites showed almost irreversible chemisorption—Br<sub>2</sub> recovery was only up to 10%. After thermal desorption of Br<sub>2</sub> from both POCs, halogen compounds such as ionized bromine atoms (<sup>79</sup>Br<sup>+</sup>, <sup>81</sup>Br<sup>+</sup>) and hydrogen bromide ions (<sup>1</sup>H<sup>79</sup>Br<sup>+</sup>, <sup>1</sup>H<sup>81</sup>Br<sup>+</sup>) were identified by coupling the evolved gas analyzer with a mass spectrometer (**Fig. S6 and S7†**). The time-intensity curve (TIC) tailing was longer in FT-RCC3 with significantly delayed desorption behavior, implying the increased number of residual bromine compounds trapped in FT-RCC3. For FT-RCC3, a considerable fraction of the Br<sub>2</sub> remained within the interior cavity, and would not be desorbed by heat treatment due to a strong interaction with host cages, resulting in almost irreversible chemisorption.

The PXRD patterns of the CC3-R and FT-RCC3 after sorption-desorption measurement of Br<sub>2</sub> have confirmed that POCs lost their crystal packing (**Fig. S8†**), most likely due to the preferential desorption of Br<sub>2</sub> that are weakly attached to cage surface or interstitial spaces between cages. Additionally, the integrity of cage structure after Br<sub>2</sub> adsorption was confirmed by solid-state <sup>13</sup>C CPMAS NMR, X-ray Fluorescence Spectroscopy and Elemental Analysis (**Fig. S9†; Table S3 and S4†**). NMR spectra of both POCs showed broad signals after Br<sub>2</sub> adsorption, demonstrating that the captured bromine molecules impacted the mobility and chemical environment of carbon atoms.<sup>11a</sup> The new peaks at 50.97 ppm and 54.98 ppm correspond to the changes in the electromagnetic field in carbon atoms attached to N atoms due to the strong adsorption of Br<sub>2</sub> onto the N atoms, while primary aliphatic (24.97 ppm and 30.99 ppm) and aromatic (140.71 ppm) carbon structures remained unchanged. These results indicated that discrete molecular cages are modified by the interactions with bromine

molecules, resulting in the changes of structural and magnetic properties without decomposition (or destruction) of the parent unit cage structures.<sup>17</sup> After thermal treatment, the atomic compositions of “physical mixture of monomers”, which mimics the situation when the cage fragments are formed after desorption, were changed (**Table S3†**); C/N and C/H ratios were increased after thermal treatment. In contrast, the elemental compositions of POCs after bromine sorption-desorption cycle exhibited similar C/N and C/H ratios to those of pure POCs, indicating that the unit cage frameworks are nearly intact. We also confirmed that the Br/C ratio decreased after thermal desorption procedure (**Table S4†**), indicating that bromine molecules were released while the carbon composition of the cage framework was almost maintained. We determined that the Raman spectra of POCs after Br<sub>2</sub> sorption-desorption were unchanged compared to those of pure POCs; only appearance of characteristic bands of charge transfer complexes (**Fig. S10 and S11†**), while they differed from monomers (**Fig. S12†**); the characteristic bands of TFB (~ 1596 cm<sup>-1</sup> and 1688 cm<sup>-1</sup>) have not appeared at the Raman spectra of Br<sub>2</sub>@CC3-R. Additionally, we demonstrated that two POCs retained their adsorption capabilities over 5 cycles of bromine sorption-desorption procedures (**Fig. S13†**). Overall, these findings revealed that trapped bromine disrupted the regular packing of POCs, as well as

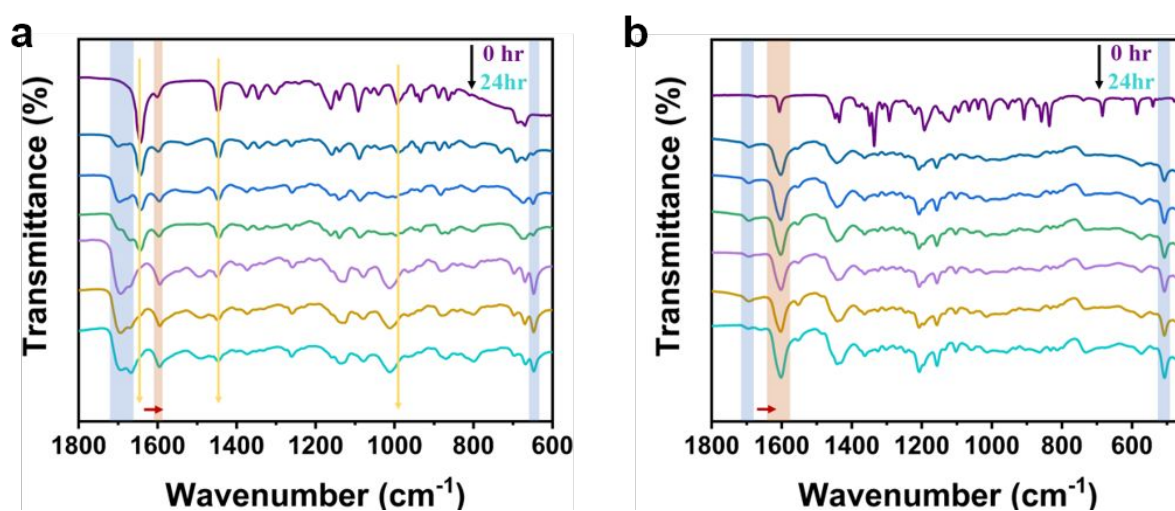


**Fig. 3** FT-IR Spectra of (a) CC3-R and (b) FT-RCC3 during static Br<sub>2</sub> adsorption at 25°C.



cage structural transformations, might have been caused by strong charge-transfer interactions, without unit cage destruction and decrease in their adsorption capabilities.

### 3.3 Br<sub>2</sub> adsorption mechanism

To support our hypothesis, we used several analyses to describe the adsorbents as synthesized (denoted as CC3-R and FT-RCC3, respectively) and after bromine capture (denoted as Br<sub>2</sub>@CC3-R and Br<sub>2</sub>@FT-RCC3, respectively). Time-resolved FT-IR spectra showed that during Br<sub>2</sub> adsorption, Br<sub>2</sub>@CC3-R exhibited reduced intensities in the -C=N- bond at 1643 cm<sup>-1</sup>, C-N bond at 1160 cm<sup>-1</sup>, and C-H bond bands at 1445 and 990 cm<sup>-1</sup>; additionally, the peak associated with the C=C bond at 1600 cm<sup>-1</sup> underwent a gradual redshift<sup>8, 13c, 18</sup> (Fig. 3a). Some new vibration bands emerged at 647 cm<sup>-1</sup> and in the range of 1668–1698 cm<sup>-1</sup>

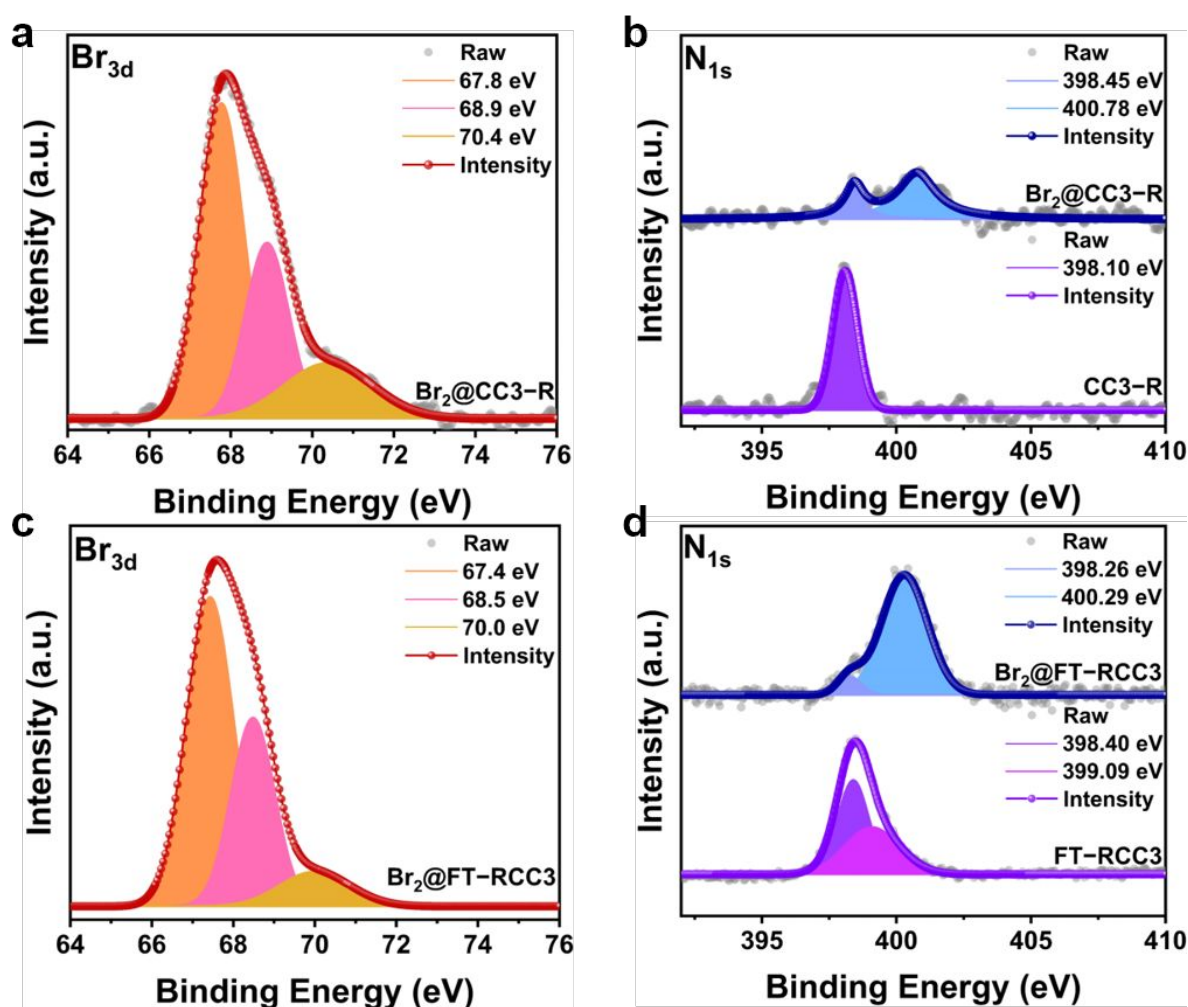


**Fig. 4.** XPS spectra of bromine captured POCs. Br<sub>3d</sub> XPS spectra of (a) Br<sub>2</sub>@CC3-R and (c) Br<sub>2</sub>@FT-RCC3. N<sub>1s</sub> XPS spectra of (b) pristine CC3-R and Br<sub>2</sub>@CC3-R and (d) pristine FT-RCC3 and Br<sub>2</sub>@FT-RCC3. Br<sub>2</sub> captured POCs are prepared under static conditions at 25°C and near ambient pressure and are denoted as Br<sub>2</sub>@CC3-R and Br<sub>2</sub>@FT-RCC3, respectively.



representing C–Br and N–Br interaction, respectively. In the high wavenumber range, gradual peak broadening was observed in the 2300–3200  $\text{cm}^{-1}$  region as increasing adsorption time, indicating intermolecular interaction among cyclohexane rings on the POC framework and adsorbate molecules<sup>19</sup> (**Fig. S14†**). These spectral changes implicate that the functional groups of CC3-R including imine, cyclohexane, and phenyl rings all contributed to the formation of charge-transfer complexes with bromine molecules.<sup>8</sup> For  $\text{Br}_2@FT\text{-RCC3}$ , similar results showed that all functional groups interacted with bromine molecules (**Fig. 3b** and **Fig. S15†**). The new vibration bands appeared at 507  $\text{cm}^{-1}$  and 1694  $\text{cm}^{-1}$  representing C-Br and N-Br bonds, respectively. The peak assigned to C=C bond at 1607  $\text{cm}^{-1}$  underwent a gradual redshift, also suggesting the existence of charge-transfer interactions between host cages and guest bromine molecules in FT-RCC3.

X-ray photoelectron spectroscopy (XPS) was used to precisely measure the atomic states of the trapped bromine species. The  $\text{Br}_{3d}$  spectra revealed the two major component peaks, which were attributed to the physisorbed bromine species including  $\text{Br}_2$  molecule and bromine derivatives such as Br and HBr (68.9 eV and 70.4 eV) and bromine molecules adsorbed with host cages as charge-transfer complexes<sup>20</sup> (67.8 eV) (**Fig. 4a**). These findings

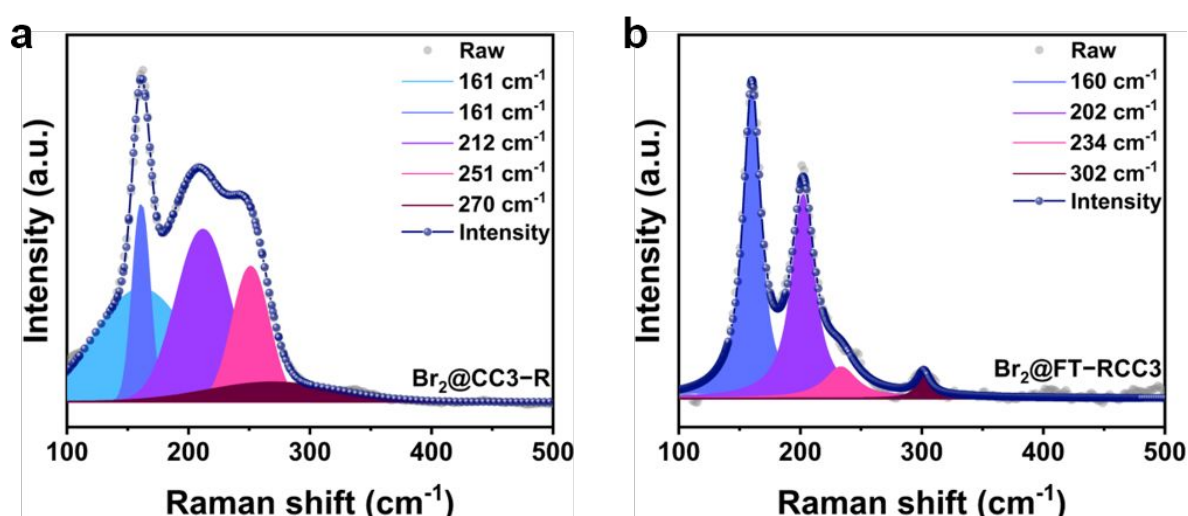


**Fig. 5** Raman spectra of (a)  $\text{Br}_2@CC3\text{-R}$  and (b)  $\text{Br}_2@FT\text{-RCC3}$ .

were further supported by the  $\text{Br}_{3p}$  spectra showing the characteristic peak of charge-transfer complexes (181.1 eV and 187.2 eV) (**Fig. S16†**). Furthermore, the adsorption of  $\text{Br}_2$  at CC3-R caused a blue shift from 398.10 eV to 398.45 eV in the  $\text{N}_{1s}$  spectra (**Fig. 4b**), suggesting that all N atoms in the cage interacted with  $\text{Br}_2$ .<sup>8</sup> The new peak at 400.78 eV is associated with N–Br bond<sup>21</sup> of the charge-transfer complexes between imine linkage of CC3-R and  $\text{Br}_2$ . The  $\text{C}_{1s}$  spectra (**Fig. S17†**) also showed a peak shift from 284.24 eV to 284.35 eV, indicating its interaction with bromine, which was consistent with previous FT-IR results (**Fig. 3a**). In the case of FT-RCC3, similar findings were obtained in all of the XPS elements (**Fig. 4c and 4d; Fig. S16 and S17†**). The  $\text{Br}_{3d}$  spectra also showed peaks of two major components, including physisorbed bromine species (68.5 eV and 70.0 eV) and bromine adsorbed as charge-transfer complexes (67.4 eV). The  $\text{N}_{1s}$  and  $\text{C}_{1s}$  XPS spectra of  $\text{Br}_2$ @FT-RCC3 revealed peak shifts of all  $\text{N}_{1s}$  and  $\text{C}_{1s}$  peaks, indicating their strong interactions with bromine molecules. These results clearly demonstrated that the trapped bromine molecules interacted with host cages, particularly at the N atomic sites, forming charge-transfer complexes.

We further employed Raman spectroscopy to identify adsorbed bromine species (**Fig. 5a and 5b; Fig. S18†**). Unlike pure  $\text{Br}_2$  vapor represented by the single Raman band at  $323\text{ cm}^{-1}$ ,<sup>22</sup>  $\text{Br}_2$ @CC3-R showed four bands at  $161\text{ cm}^{-1}$ ,  $212\text{ cm}^{-1}$ ,  $251\text{ cm}^{-1}$ , and  $270\text{ cm}^{-1}$ . These bands are associated with symmetric stretching vibration of polybromide  $\text{Br}_3^-$  ( $161\text{ cm}^{-1}$ ), asymmetric stretching vibration of polybromide  $\text{Br}_3^-$  and  $\text{Br}_5^-$  ( $212\text{ cm}^{-1}$ ), symmetric stretching vibration of polybromide  $\text{Br}_5^-$  and  $\text{Br}_2$  molecule which have confinement effect ( $251\text{ cm}^{-1}$ ), and symmetric stretching vibration of concerted  $\text{Br}_2$  molecule ( $270\text{ cm}^{-1}$ ),<sup>23</sup> respectively. Similarly,  $\text{Br}_2$ @FT-RCC3 presented two bands that showed high intensity at  $160\text{ cm}^{-1}$  and  $202\text{ cm}^{-1}$ , associated with symmetric stretching vibration of polybromide  $\text{Br}_3^-$ , asymmetric stretching vibration of polybromide  $\text{Br}_3^-$ ,<sup>24</sup> and the other two bands which exhibited relatively low intensity at  $234\text{ cm}^{-1}$  and  $302\text{ cm}^{-1}$ , associated with symmetric stretching vibration of intercalated  $\text{Br}_2$  molecule,

and symmetric stretching vibration of Br<sub>2</sub> molecule at condensed phase,<sup>23b, 24</sup> respectively. These findings demonstrated that bromine molecules could exist in porous organic cages as both polybromide species (Br<sub>3</sub><sup>-</sup>, Br<sub>5</sub><sup>-</sup>) and pure bromine molecules; specifically, polybromide species dominated. Notably, the characteristic band of Br<sub>5</sub><sup>-</sup> was only identified at CC3-R, indicating that the formation of Br<sub>5</sub><sup>-</sup> in FT-RCC3 would be unfavorable due to the steric hindrance effect caused by the tied-methylene group. It is also worth noting that Br<sub>3</sub><sup>-</sup> with FT-RCC3 has larger adsorption energy than Br<sub>3</sub><sup>-</sup> and Br<sub>5</sub><sup>-</sup> with CC3-R (**Table S5†**), which means that polybromide species in CC3-R could be desorbed more easily, resulting in better reversibility than FT-RCC3.

### 3.4 Computational studies of Br<sub>2</sub> adsorbed POCs

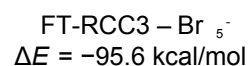
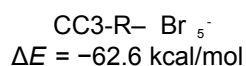


**Fig. 6** Optimized structures of CC3-R and FT-RCC3 with adsorbed polybromide Br<sub>5</sub><sup>-</sup>. All energies are relative to free POCs and 3 bromine molecules.

Additionally, we computed the vibrational frequencies of isolated Br<sub>n</sub> (n=2, 3, 4, and 5) molecules as they were adsorbed inside the POC to support our experimental Raman results (detailed computational methods are discussed in the ESI†). The calculated Raman bands at

285  $\text{cm}^{-1}$  and 270  $\text{cm}^{-1}$  were observed in the case of adsorbed two  $\text{Br}_2$  and three  $\text{Br}_2$  molecules, respectively for the CC3 cage (**Fig. S28** and **S29†**). These Raman bands correspond to the experimentally observed Raman bands for CC3 ( $\sim 251 \text{ cm}^{-1}$  and  $270 \text{ cm}^{-1}$ ). Since the simulated Raman peaks typically redshift to 10 – 20  $\text{cm}^{-1}$  (see **Table S7†**), it is reasonable to conclude that the experimentally observed Raman peaks correspond to the concerted vibration of  $\text{Br}_2$  molecules within the cage. However, we were not able to resolve the origin of the largest intensity peak ( $\sim 160 \text{ cm}^{-1}$ ) observed in the experiments. Since our calculations involve a single cage, we speculate that these peaks originate from the  $\text{Br}_2$  molecules that are adsorbed between the cages, indicating that the formation of polybromide species is mainly affected by the presence of intermolecular pores of POCs. It was also reported that the vibration frequency of Br-Br bond,  $\omega_{\text{Br}-\text{Br}}$ , was strongly affected by the external environment and charge density state (e.g. intermolecular interaction between bromine chains and that between chains and host cages).<sup>23</sup> In this regard, as the number of molecules in the cage increased, the bromine molecule would have a highly confined effect, resulting in a redshift of its Raman band. These calculated vibrational frequencies were in good agreement with our experimental Raman bands and previous studies.<sup>23, 24</sup>

To better understand of the mechanism of charge-transfer complex formation and physicochemical states of bromine species, DFT calculations were carried out to compute the binding and formation energies as a function of bromine species and the number of unreacted bromine molecules within the two cages. The calculated adsorption energies between CC3-R and  $\text{Br}_3^-$  are 33.9 kcal/mol and binding energies between FT-RCC3 and  $\text{Br}_3^-$  are 74.0 kcal/mol, respectively (**Fig. 6** and **Table S5†**). The differences in the adsorption energies of both POCs indicate the difficulty of desorbing the adsorbed bromine species in CC3-R and FT-RCC3, which is likely the culprit of the irreversible desorption of bromine species from FT-RCC3. The binding energy of the first bromine molecule is more favorable with FT-RCC3 when

compared to CC3-R, which is primarily facilitated through stronger electrostatic interactions (**Table S6†**). These calculation results provide a reasonable explanation for the faster Br<sub>2</sub> uptake kinetics of FT-RCC3 than CC3-R at lower adsorption time (< 12 hours). However, the binding of additional bromine molecules is more favored with CC3-R, which can form strong halogen bonding interactions with imine nitrogen, increasing charge transfer interactions (**Fig. S31†**), and leading to a short N...Br interatomic distance (**Fig. S33A†**). On the other hand, FT-RCC3 is primarily stabilized through additional C-H...Br through-space interactions. These are facilitated through two distinct orbital interactions. First, lone pair- $\sigma^*$  interactions between tertiary amine and bromine molecule are still present with FT-RCC3 but occur through hyperconjugation of nitrogen lone pair to energetically less favorable C-H  $\sigma^*$  orbital due to diminished orbital overlap (**Fig. S32†**). Additional charge-transfer interactions between bromine lone pair (lp) and “tying” C-H  $\sigma^*$  are also present which is unique to FT-RCC3 and leads to additional stabilization. These factors together lead to a longer N...Br interatomic distance and a shorter H...Br interatomic distance. Furthermore, due to the presence of lp  $\rightarrow$   $\sigma^*$  interactions, there is a significant elongation of the tying C-H bond (**Fig. S33B†**), which can promote the deprotonation and HBr formation with FT-RCC3. Therefore, FT-RCC3 can form significantly more stable polybromide species, through more favorable deprotonation of the “tying” methylene group (**Fig. S30†**). We hypothesized that the tied-methylene groups in FT-RCC3 decrease the mobility of trapped bromine species in the host cages, resulting in more stable storage of bromine in polybromide species forms that are not easily desorbed. For CC3-R, bromine species can move more freely in the cage structure compared to FT-RCC3. DFT calculation results provide additional support for this hypothesis. We found that the calculated formation energy of carbocation species (Br<sub>3</sub><sup>-</sup> and Br<sub>5</sub><sup>-</sup>) is significantly more exergonic for FT-RCC3 than it is for CC3-R. Based on these calculations, we conclude that HBr and Br<sub>5</sub><sup>-</sup> species are the most energetically stable species compared with other bromine species. This is

consistent with experimental Raman spectra analyses that bromine molecules would mainly exist as polybromide states (**Fig. 5a** and **5b**), and EGA-MS analysis which showed that the hydrogen bromide was detected at both POCs after the thermal treatment process (**Fig. S6** and **S7†**).

## 4 Conclusion

In this work, we present the new application of porous organic cages as potential candidates for highly toxic and volatile Br<sub>2</sub> vapor capture. For efficient bromine capture, it should be considered several factors including textural properties, affinity with bromine molecules and densities of binding sites. Two different N-containing POCs (CC3-R and FT-RCC3), which have high porosity and many favorable binding sites for Br<sub>2</sub>, show high Br<sub>2</sub> vapor capture performance under static conditions. FT-RCC3, which has a lower total pore volume, exhibits a faster bromine adsorption kinetics than CC3-R with similar adsorption capacities, indicating that affinity between host materials and guest molecules is the critical factor for enhancing capture performance. Interestingly, both POCs showed different desorption abilities owing to their structural difference. DFT calculation results show that the formation of carbocationic species (Br<sub>3</sub><sup>-</sup> and Br<sub>5</sub><sup>-</sup>) and HBr is energetically more favorable within the cage. The energy decomposition analyses showed that both POCs showed highly stabilizing halogen bonding interaction with bromine. This study demonstrates the essential role of strong host-guest interaction in the development of highly efficient capture and storage performance adsorbents. We believe that these N-containing POCs, coupled with their good processability and synthetic scalability, can be utilized for toxic and volatile halogen vapor capture.

### Corresponding Author

\* E-mail : [greg.chung@pusan.ac.kr](mailto:greg.chung@pusan.ac.kr), [dongyeunkoh@kaist.ac.kr](mailto:dongyeunkoh@kaist.ac.kr)

### Author Contributions

All authors have approved the final version of the manuscript. / ‡These authors contributed equally.

### Conflict of interest

The authors declare no competing financial interest.

### Acknowledgements

This work was supported by the “2021 Joint Research Project of Institutes of Science and Technology” and the National Research Foundation of Korea (NRF) funded by the Ministry of Science and ICT (NRF-2021R1C1C1012014). This work was partially supported (to H.J.K. and I.K.) by the NSF Center for the Chemistry of Molecularly Optimized Networks (MONET), CHE-2116298. This work was also partly supported by the C1 Gas Refinery Program through the National Research Foundation of Korea (NRF) funded by the Ministry of Science and ICT (NRF-2018M3D3A1A01055761 and NRF-2021M3D3A1A0102210431)

### References

- 1 G. L. Soloveichik, Metal-free energy storage, *Nature*, 2014, **505**, 163–165.
- 2 C. Wang, Q. Lai, K. Feng, P. Xu, X. Li, H. Zhang, From zeolite-type metal organic framework to porous nano-sheet carbon: High activity positive electrode material for bromine-based flow batteries, *Nano Energy*, 2018, **44**, 240–247.
- 3 a) Y. Tulchinsky, C. H. Hendon, K. A. Lomachenko, E. Borfecchia, B. C. Melot, M. R. Hudson, J. D. Tarver, M. D. Korzyński, A. W. Stubbs, J. J. Kagan, C. Lamberti, C. M. Brown, M. Dincă, Reversible Capture and Release of Cl<sub>2</sub> and Br<sub>2</sub> with a Redox-

- Active Metal-Organic Framework, *J. Am. Chem. Soc.*, 2017, **139**, 5992–5997. b) J. Pang, S. Yuan, D. Du, C. Lollar, L. Zhang, M. Wu, D. Yuan, H.-C. Zhou, M. Hong, Flexible Zirconium MOFs as Bromine Nanocontainers for Bromination Reactions under Ambient Conditions, *Angew. Chem. Weinheim Bergstr. Ger.*, 2017, **129**, 14814–14818.
- 4 a) Y.-P. Lin, B. Xia, S. Hu, Y. Zhong, Y.-E. Huang, Z.-Z. Zhang, N. Wu, Y.-W. Wu, X.-H. Wu, X.-Y. Huang, Z. Xiao, K.-Z. Du, Reversible Release and Fixation of Bromine in Vacancy-Ordered Bromide Perovskites, *Energy Environ. Mater.*, 2020, **3**, 535–540. b) Y.-P. Lin, X.-Y. Huang, K.-Z. Du, Br<sub>2</sub>-free method for XBr<sub>3</sub> (X= Cs, C<sub>8</sub>H<sub>20</sub>N, C<sub>16</sub>H<sub>36</sub>N) synthesis: Br<sub>2</sub> solid storage and separation from aqueous solution, *Mater. Chem. Phys.*, 2022, **280**, 125820.
- 5 L. He, L. Chen, X. Dong, S. Zhang, M. Zhang, X. Dai, X. Liu, P. Lin, K. Li, C. Chen, T. Pan, F. Ma, J. Chen, M. Yuan, Y. Zhang, L. Chen, R. Zhou, Y. Han, Z. Chai, S. Wang, *Chem* **2021**, *7*, 699–714.
- 6 C. Wang, Y. Wang, R. Ge, X. Song, X. Xing, Q. Jiang, H. Lu, C. Hao, X. Guo, Y. Gao, D. Jiang, A nitrogen-rich covalent organic framework for simultaneous dynamic capture of iodine and methyl iodide, *Chemistry*, 2018, **24**, 585–589.
- 7 a) M. Xu, T. Wang, L. Zhou, D. Hua, Fluorescent conjugated mesoporous polymers with N,N-diethylpropylamine for the efficient capture and real-time detection of volatile iodine, *J. Mater. Chem. A Mater. Energy Sustain.*, 2020, **8**, 1966–1974. b) T.-H. Niu, C.-C. Feng, C. Yao, W.-Y. Yang, Y.-H. Xu, Bismidazole-based conjugated polymers for excellent iodine capture, *ACS Appl. Polym. Mater.*, 2021, **3**, 354–361.
- 8 Y. Xie, T. Pan, Q. Lei, C. Chen, X. Dong, Y. Yuan, J. Shen, Y. Cai, C. Zhou, I. Pinnau, Y. Han, Ionic Functionalization of Multivariate Covalent Organic Frameworks to



- Achieve an Exceptionally High Iodine-Capture Capacity, *Angew. Chem. Int. Ed Engl.*, 2021, **60**, 22432–22440.
- 9 a) S. Salai Cheettu Ammal, S. P. Ananthavel, P. Venuvanalingam, M. S. Hegde\*, UVPES and ab Initio Molecular Orbital Studies on the Electron Donor-Acceptor Complexes of Bromine with Methylamines, *J. Phys. Chem. A*, 1997, **101**, 1155–1159.  
b) M. M. Naseer, A. Bauzá, H. Alnasr, K. Jurkschat, A. Frontera, Lone pair- $\pi$  vs  $\sigma$  hole- $\pi$  interactions in bromine head-containing oxacalix[2]arene[2]triazines, *CrystEngComm*, 2018, **20**, 3251–3257.
- 10 a) L. Chen, P. S. Reiss, S. Y. Chong, D. Holden, K. E. Jelfs, T. Hasell, M. A. Little, A. Kewley, M. E. Briggs, A. Stephenson, K. M. Thomas, J. A. Armstrong, J. Bell, J. Busto, R. Noel, J. Liu, D. M. Strachan, P. K. Thallapally, A. I. Cooper, Separation of rare gases and chiral molecules by selective binding in porous organic cages, *Nat. Mater.*, 2014, **13**, 954–960. b) M. Brutschy, M. W. Schneider, M. Mastalerz, S. R. Waldvogel, Porous organic cage compounds as highly potent affinity materials for sensing by quartz crystal microbalances, *Adv. Mater.*, 2012, **24**, 6049–6052. c) X. Yang, J.-K. Sun, M. Kitta, H. Pang, Q. Xu, Encapsulating highly catalytically active metal nanoclusters inside porous organic cages, *Nature Catalysis*, 2018, **1**, 214–220. d) T. Mitra, K. E. Jelfs, M. Schmidtman, A. Ahmed, S. Y. Chong, D. J. Adams, A. I. Cooper, Molecular shape sorting using molecular organic cages, *Nat. Chem.*, 2013, **5**, 276–281.
- 11 a) E. Martínez-Ahumada, D. He, V. Berryman, A. López-Olvera, M. Hernandez, V. Jancik, V. Martis, M. A. Vera, E. Lima, D. J. Parker, A. I. Cooper, I. A. Ibarra, M. Liu, SO<sub>2</sub> Capture Using Porous Organic Cages, *Angew. Chem. Int. Ed Engl.*, 2021, **60**, 17556–17563. b) T. Hasell, M. Schmidtman, A. I. Cooper, Molecular doping of porous organic cages, *J. Am. Chem. Soc.*, 2011, **133**, 14920–14923.

- 12 a) M. Liu, L. Zhang, M. A. Little, V. Kapil, M. Ceriotti, S. Yang, L. Ding, D. L. Holden, R. Balderas-Xicohténcatl, D. He, R. Clowes, S. Y. Chong, G. Schütz, L. Chen, M. Hirscher, A. I. Cooper, Barely porous organic cages for hydrogen isotope separation, *Science*, 2019, **366**, 613–620. b) M. Liu, M. A. Little, K. E. Jelfs, J. T. A. Jones, M. Schmidtman, S. Y. Chong, T. Hasell, A. I. Cooper, Acid- and base-stable porous organic cages: shape persistence and pH stability via post-synthetic “tying” of a flexible amine cage, *J. Am. Chem. Soc.*, 2014, **136**, 7583–7586.
- 13 a) T. Hasell, S. Y. Chong, K. E. Jelfs, D. J. Adams, A. I. Cooper, Porous organic cage nanocrystals by solution mixing, *J. Am. Chem. Soc.*, 2012, **134**, 588–598. b) M. E. Briggs, A. G. Slater, N. Lunt, S. Jiang, M. A. Little, R. L. Greenaway, T. Hasell, C. Battilocchio, S. V. Ley, A. I. Cooper, Dynamic flow synthesis of porous organic cages, *Chem. Commun.*, 2015, **51**, 17390–17393. c) J. Lucero, C. Osuna, J. M. Crawford, M. A. Carreon, Microwave-assisted synthesis of porous organic cages CC3 and CC2, *CrystEngComm*, 2019, **21**, 4534–4537. d) B. D. Egleston, M. C. Brand, F. Greenwell, M. E. Briggs, S. L. James, A. I. Cooper, D. E. Crawford, R. L. Greenaway, Continuous and scalable synthesis of a porous organic cage by twin screw extrusion (TSE), *Chem. Sci.*, 2020, **11**, 6582–6589.
- 14 T. Tozawa, J. T. A. Jones, S. I. Swamy, S. Jiang, D. J. Adams, S. Shakespeare, R. Clowes, D. Bradshaw, T. Hasell, S. Y. Chong, C. Tang, S. Thompson, J. Parker, A. Trewin, J. Bacsá, A. M. Z. Slawin, A. Steiner, A. I. Cooper, Porous organic cages, *Nat. Mater.*, 2009, **8**, 973–978.
- 15 S.-L. Zheng, Y. He, X.-K. Qiu, Y.-H. Zhong, L.-H. Chung, W.-M. Liao, J. He, Synthesis, structures and Br<sub>2</sub> uptake of Cu(I)-bipyrazole frameworks, *J. Solid State Chem.*, 2021, **302**, 122458.

- 16 a) H. Wang, A. Zhou, F. Peng, H. Yu, J. Yang, Mechanism study on adsorption of acidified multiwalled carbon nanotubes to Pb(II), *J. Colloid Interface Sci.*, 2007, **316**, 277–283. b) Y. Liu,, New insights to pseudo-second-order kinetic equation for adsorption, *Colloids Surf. A Physicochem. Eng. Asp.*, 2008, **320**, 275–278.
- 17 a) K. Takai, H. Kumagai, H. Sato, T. Enoki, Bromine-adsorption-induced change in the electronic and magnetic properties of nanographite network systems, *Phys. Rev. B Condens. Matter*, 2006, **73**, 035435. b) H. Sato, N. Kawatsu, T. Enoki, M. Endo, R. Kobori, S. Maruyama, K. Kaneko, Drastic effect of water-adsorption on the magnetism of carbon nanomagnets, *Solid State Commun.*, 2003, **125**, 641–645.
- 18 a) Q. Song, W. D. Wang, X. Hu, Z. Dong, Ru nanoclusters confined in porous organic cages for catalytic hydrolysis of ammonia borane and tandem hydrogenation reaction, *Nanoscale*, 2019, **11**, 21513–21521. b) T. Gelles, A. A. Rownaghi, F. Rezaei, Diffusion Kinetics of CO<sub>2</sub>, CH<sub>4</sub>, and their Binary Mixtures in Porous Organic Cage CC3, *J. Phys. Chem. C*, 2019, **123**, 24172–24180.
- 19 a) C. A. Coulson, G. N. Robertson, A Theory of the Broadening of the Infrared Absorption Spectra of Hydrogen-Bonded Species. II. The Coupling of Anharmonic  $\nu$  (XH) and  $\nu$  (XH..Y) Modes, *Proc. R. Soc. Lond. A Math. Phys. Sci.*, 1975, **342**, 289–315. b) G. R. Satyanarayana, D. B. K. Kumar, K. Sujatha, Probing the intermolecular interactions in the binary liquid mixtures of o-chlorophenol with alkoxyethanols through ultrasonic, transport and FT-IR spectroscopic studies at different temperatures, *Journal of Molecular Liquids*, 2016, **216**, 526-537.
- 20 a) L. G. Bulusheva, A. V. Okotrub, E. Flahaut, I. P. Asanov, P. N. Gevko, V. O. Koroteev, Y. V. Fedoseeva, A. Yaya, C. P. Ewels, Bromination of double-walled carbon nanotubes, *Chem. Mater.*, 2012, **24**, 2708–2715. b) I. Mazov, D. Krasnikov, A. Stadnichenko, V. Kuznetsov, A. Romanenko, O. Anikeeva, E. Tkachev, Direct vapor-

- phase bromination of multiwall carbon nanotubes, *J. Nanotechnol.*, 2012, 2012, DOI 10.1155/2012/954084. c) E. Papirer, R. Lacroix, J.-B. Donnet, XPS Study of the halogenation of carbon black-part 1. Bromination, *Carbon N. Y.*, 1994, **32**, 1341–1358.
- 21 H. S. O. Chan, H. S. Munro, C. Davies, E. T. Kang, XPS studies of chemically synthesized polypyrrole-halogen charge transfer complexes, *Synth. Met.*, 1988, **22**, 365–370.
- 22 a) J. E. Cahill, G. E. Leroi, Raman spectra of solid chlorine and bromine, *J. Chem. Phys.*, 1969, **51**, 4514–4519. b) E. T. Branigan, M. N. van Staveren, V. A. Apkarian, Solidlike coherent vibronic dynamics in a room temperature liquid: Resonant Raman and absorption spectroscopy of liquid bromine, *J. Chem. Phys.*, 2010, **132**, 044503. c) K.P. Huber, G. Herzberg, Constants of Diatomic Molecules (data prepared by J.W. Gallagher, R.D. Johnson, III) in NIST Chemistry WebBook, NIST Standard Reference Database Number 69, edited by P.J. Linstrom, W.G. Mallard, July 2001, National Institute of Standards and Technology, Gaithersburg MD, 20899 (<http://webbook.nist.gov>).
- 23 a) A. L. Aguiar, E. B. Barros, V. P. Sousa Filho, H. Terrones, V. Meunier, D. Machon, Y. A. Kim, H. Muramatsu, M. Endo, F. Baudalet, A. San-Miguel, A. G. Souza Filho, Pressure tuning of bromine ionic states in double-walled carbon nanotubes, *J. Phys. Chem. C*, 2017, **121**, 10609–10619. b) G. M. do Nascimento, T. Hou, Y. A. Kim, H. Muramatsu, T. Hayashi, M. Endo, N. Akuzawa, M. S. Dresselhaus, Double-Wall Carbon Nanotubes Doped with Different Br<sub>2</sub> Doping Levels: A Resonance Raman Study, *Nano Lett.*, 2008, **8**, 4168–4172. c) J. C. Evans, G. Y. S. Lo, Vibrational spectra of BrO<sup>-</sup>, BrO<sub>2</sub><sup>-</sup>, Br<sub>3</sub><sup>-</sup>, and Br<sub>5</sub>, *Inorg. Chem.*, 1967, **6**, 1483–1486. d) X. Chen, M. A. Rickard, J. W. Hull Jr, C. Zheng, A. Leugers, P. Simoncic, Raman spectroscopic

- investigation of tetraethylammonium polybromides, *Inorg. Chem.*, 2010, **49**, 8684–8689.
- 24 a) O. V. Sedelnikova, C. P. Ewels, D. V. Pinakov, G. N. Chekhova, E. Flahaut, A. V. Okotrub, L. G. Bulusheva, Bromine polycondensation in pristine and fluorinated graphitic carbons, *Nanoscale*, 2019, **11**, 15298–15306. b) A. Yaya, C. P. Ewels, J. K. Efavi, B. Agyei-Tuffour, K. Kan-Dapaah, B. Onwona-Agyeman, E. K. K. Abavare, A. Hassanali, P. R. Briddon, A study of polybromide chain formation using carbon nanomaterials via density functional theory approach, *Cogent Engineering*, 2016, **3**, 1261509.
- 25 Ghalami, Z, Ghoulipour, V, Khanchi, A. R. Adsorption and sequential thermal release of F<sub>2</sub>, Cl<sub>2</sub>, and Br<sub>2</sub> molecules by a porous organic cage material (CC3-R): Molecular dynamics and grand-canonical Monte Carlo simulations, *J Comput Chem*, 2020, **41**, 949-957.